ADVANCED MATERIALS INTERFACES
www.advmatinterfaces.de

Nanoscale Probing of Surface Charges in Functional Copper-Metal Organic Clusters by Kelvin Probe Force Microscopy for Field-Effect Transistors

*Rudra Kumar, Prachi Gupta, and Satinder K. Sharma**

Metal–organic frameworks (MOFs) have recently attracted a great deal of attention especially as conceivable advanced gate dielectrics for next-generation field-effect transistors (FETs) and memory device applications. Dielectric surface charge retention mapping is essential for gauging the leakage current and threshold voltage stability. Due to a dearth of systematic real-time surface charge probing of MOFs dielectrics, in this work, the nanoscale Kelvin probe force microscopy (KPFM) technique is employed for the contact potential difference (CPD) analysis of developed hybrid copper–metal–organic clusters (Cu-MOCs)/Si systems. Films are synthesized through the sol-gel process consisting of copper metal core linked with organic ligands. With 3V positive and negative DC bias, charge injection offset between positive and negative bias is observed to be ≈190 mV, indicating the intrinsic Fermi level alignment between KPFM tip and sample surface charges. The high-resolution surface CPD mappings bring forth the white (≈98 mV) and black (≈−91 mV) contrast profiles with hole (5.09×10^{12} cm^{-2}) and electron (4.74×10^{12} cm^{-2}) charge densities. Also, the 17 h time-lapse enables the holes and electrons CPD mapping diameter shrinkage by ≈32% and 46%, respectively. In furtherance, a conductive filament model for host-guest proton-assisted conduction with charge hopping through fixed/mobile ions is proposed.

1. Introduction

The emerging landscape of metal–organic frameworks (MOFs) toward a new class of functional materials for applications in gas separation, energy storage, catalysis, sensing, etc.[1–9] has attracted immense attention by the scientific community for decades. However, MOFs are versatile materials because of their physical, chemical, and structural tunability, excelling in chemical applications. Conversely, MOFs also reveal prospective scope in the futuristic electronic,[10–13] ferromagnetic,[14] electrolytic,[15] piezoelectric,[16] ferrorelectric,[16] photonic,[17] photovoltaic device applications. Indeed, the next-generation electronic device applications require high-quality semiconducting materials,[18] ferroelectric materials,[19] ferromagnetic materials,[20] and compatible high-κ dielectrics.[12] In this context, high-speed electronics and power-efficient devices necessitate the advances in semiconductor materials[3,12] and replacing conventional insulating interfaces with novel high-κ dielectrics.[11] MOFs based high-κ dielectric can prove to be essential for various applications such as field-effect transistor (FET),[22] charge and non-charge storage memories,[21] and other electronic device applications. FETs comprising metal–insulator–metal,[12] metal–insulator–semiconductor (MIS)[23] structures, MISFETs,[24] tunnel FETs,[25] organic-FETs,[26] Fin-FETs,[27] quantum tunnel junctions, advanced sensing[28] electronic device applications. MIS capacitor is an indispensable part of MISFETs, which require high capacitance, lower leakage currents, higher charge retention, etc. On the other hand, memory applications: NAND, NOR FLASH and ferroelectric RAM (FeRAM), magnetic RAM, phase change RAM and resistive RAM (ReRAM), etc.[29–32] Applications such as NVM applications require much thicker dielectrics with much longer charge storage properties at favorable trap sites. Hence, MOSFETs are essentially potential applications for MOF-based high-κ dielectric materials. In advanced electronic devices, dielectrics are used as active device materials and as passive materials such as interfacial layer engineering, electrical passivation in electronic devices, interlayer dielectric, and so on.[33,34] Hence, novel dielectrics, especially hybrid MOFs based high-κ dielectrics, find numerous applications in electronics, opto-electronics,[35] photovoltaic[36] devices for next-generation technology nodes. Indeed, cost-effective process and high-quality large surface area thin film formation in MOFs dielectric materials promise to explore a new arena as a possible alternate high-κ dielectrics for hyper-scaled silicon or analogous FETs technology.[37–41]

Most of the existing MOFs in literature are known for their dielectric nature depicting especially low-κ, ultralow-κ, and also, on the other hand, high-κ properties. For instance, Usman et al.[33] reviewed MOFs as new interlayer dielectrics,

R. Kumar, P. Gupta, S. K. Sharma
School of Computing and Electrical Engineering (SCEE)
Indian Institute of Technology (IIT)-Mandi
Mandi, Himachal Pradesh 175075, India
E-mail: satinder@iitmandi.ac.in

The ORCID identification number(s) for the author(s) of this article can be found under https://doi.org/10.1002/admi.202100529.

DOI: 10.1002/admi.202100529

and Galli et al.[42] presented fluorous MOFs as a low-κ dielectric. It is accomplished that Zr-based MOFs are primarily identified as inherently insulating, even despite of electroactive guests inclusion.[43,44] Pathak et al.[11] reported high-κ dielectric samarium-based MOF for gate applications. Usman et al.[45] also showcase high-κ dielectric Sr-MOF with dielectric modulation based on polar molecule confinement. For a while, Engelbert Redel et al.[46] demonstrated the dielectric and optical properties of MOFs thin films.

Nevertheless, with the successive approach toward shrinking technology nodes (down to a few nm) and the gate dielectric thickness scaling down (<1 nm) to the nanoscale regime in complementary metal–oxide–semiconductor (CMOS) technology, new concerns arose requiring victorious solutions for MISFETs. Conventionally, the properties of a potential dielectric material used for transistor application have typically been investigated long ago by macroscopic probing techniques.[47,48] However, as the dimension of the next-generation FETs is continuously scaled-down, macroscopic probing results in being insensitive to charge variations, especially at the nanoscale regime. Hence, there is a need for more precise and robust nano-scale probing solutions to characterize next-generation devices such as quantum tunnel junctions.

This requires a high-resolution, non-destructive characterization technique that can proficiently inspect highly localized charge retention, decay analysis, and retention ability about the surface potential (CPD) of the dielectrics.[49–52] Furthermore, understanding surface charges build-up and transport in the dielectric are crucial and desirable for performance improvement and reliability of the FETs such as MISFETs, tunnel FETs FinFETs, and memories such as FeRAM, NVM, and ReRAM. The charge retention ability of dielectrics is essential for establishing the leakage current and threshold voltage instability in gate dielectrics for MISFETs, charge storage memories, etc. Notwithstanding, charge retention is greatly impacted by the gate dielectrics thickness and the presence of intrinsic traps/defects.[53]

Recently, atomic force microscopy (AFM) is an imaging technique increasingly used to map surface charges in thin dielectric films, such as SPM,[54] EFM, and KPFM.[55] Here, the less-explored reign of dielectric is nanoscale probing through the facile Kelvin probe force microscopy (KPFM).[55,56] Although, there are a large variety of samples and devices such as conducting polymer, metals, semiconductor devices, Langmuir–Blodgett films, nanoscale photovoltaic mapping,[57] solar cells,[58] memory devices,[59] electrical properties of the functional materials,[60] surface potential of biomolecules,[61] triboelectric nanogenerators,[62] direct determination of density of states,[63] and so on have been analyzed in recent past through KPFM, and established the corresponding contact potential analysis.[64,65] As well, KPFM, also has adequate strength for broad applications in investigating the charge dynamics in ferroelectric and dielectric systems.[66]

Indeed, KPFM is a non-destructive technique that can measure metal's local work function (φS), the dopant concentration in semiconductors, and fixed charges at the surface and bulk of an insulator in non-contact mode along with high spatial resolution.[67] Although, based on the Kelvin method, KPFM records the nanoscale electrostatic-force interaction between the highly sensitive atomically cantilever and the sample surface instead of measuring AC flow. A Kelvin electrode is simply a conducting probe tip with DC bias and AC power supplies to introduce alternating force components in the cantilever. The characterization, especially with this advanced KPFM technique, helps to find out local electronic structural properties and trap sites of ultra-thin dielectrics at the nanoscale regime without any direct contact between electrode and sample surface. Hence, the KPFM study is the best choice for the analysis of fragile and soft hybrid MOFs systems.

In contrast to frequency-modulated KPFM, AM-KPFM provides much higher sensitivity, led by lower application voltages. Also, AM-KPFM in lift mode is more benefited due to the decoupling of its electrostatic responses from any other short-ranged forces that act on the tip during tapping motion.[68] Hence, AM-KPFM is the best-suited technique for electrostatic measurements for copper metal–organic clusters (Cu-MOCs) thin-films/silicon systems. In the recent past, KPFM is also used to measure the density of states to the organic semiconductor channel on top of the dielectric layer to FETs systems.[63] Dumus and co-workers studied the charge injection and diffusion behavior between silicon nanocrystals embedded SiO_2 using the KPFM method.[69] Xu and co-workers reported the charge injection and transportation process in Si-nanocrystal-based sandwiched structure using KPFM and conductive AFM to quantify the charge density and decay mechanism.[70] Another work showed the use of KPFM for the charge trapping in phosphorous doped Si-nanocrystals and charge transfer between Si-nanocrystals and Si substrates.[71]

For the first time, copper-based MOCs dielectrics were synthesized through the facile sol–gel process. The functionalized Cu-MOCs with good solubility in organic solvents and excellent thin-film formation properties were used to form Cu-MOCs/Si structures. The nanoscale localized mapping of surface charges retention and decay analysis was conducted on Cu-MOCs/Si structures through non-destructive KPFM probing. In this investigation, the charges were injected on top of functionalized Cu-MOCs thin films and then followed by subsequent surface mapping in non-contact AFM mode of Cu-MOCs/Si systems to analyze a reliable alternate gate dielectric for CMOS technology-based advanced electronic devices such as FETs.

2. Experimental Section

2.1. Materials

Copper acetate, triethylamine, and ethyl acetate were purchased from SD Fine Chemicals. M-toluic acid was purchased from Merck. Ethyl lactate was bought from TCI Chemicals. Silicon wafers were purchased from the Wafer World.

2.2. Cu-MOCs Material Synthesis

Briefly, copper acetate was dispersed in ethyl acetate solution to form solution A. After that 490 mg of M-toluic acid, 1.5 mL of ethyl acetate, and 280 mg of triethylamine were mixed to form solution B. Then, solution B was slowly added with constant stirring into solution A at 65 °C constant temperature.

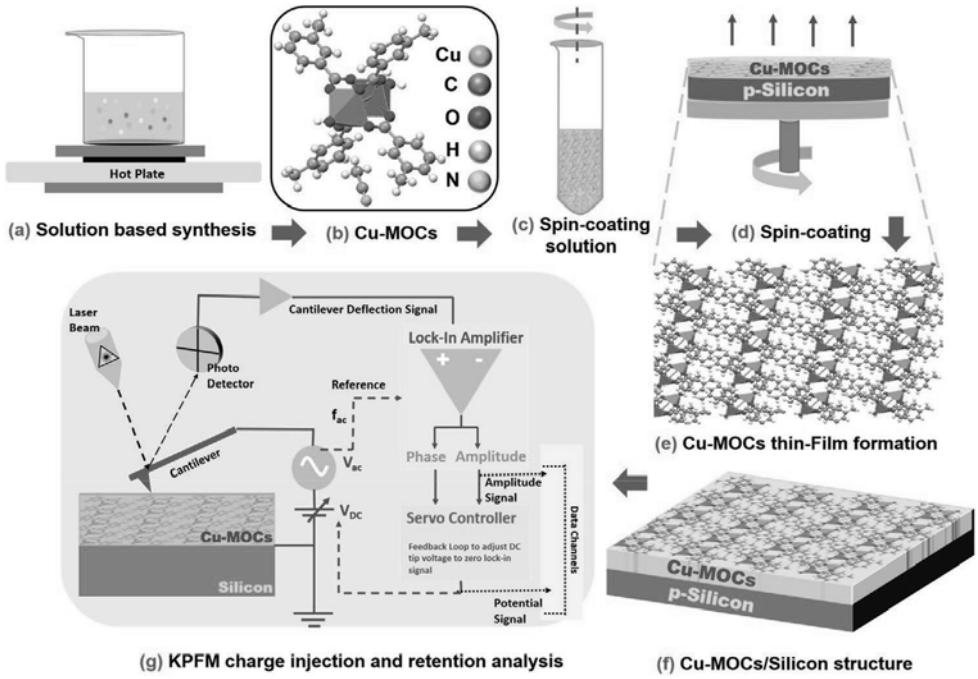

Figure 1. Fabrication schematic flow and nano-probe KPFM setup for Cu-MOCs/Si structures. a) Solution-based synthesis of Cu-MOCs material. b) A representative Cu-MOC structure comprising Cu, C, O, H, N atoms. c) Cu-MOCs spin-coating solution formulation. d) Spin coating of Cu-MOCs. e) Cu-MOCs thin-film formation. f) As-fabricated resultant Cu-MOCs/Silicon structure. g) KPFM characterization setup for surface charge injection, and retention analysis.

Additionally, 1.5 mL of ethyl acetate was added to this solution, and the above temperature was maintained for 24 h. After the completion of the reaction, the product was washed with ethanol and dried for 10 h in a vacuum oven at 60 °C constant temperature. Also, single crystals of Cu-MOCs were grown by dissolving 10 wt% of Cu-MOCs in acetonitrile solvent and keeping the solution undisturbed for 7 days at room temperature. Cu-MOCs were synthesized through the facile sol–gel, low-temperature, and cost-efficient synthesis method as shown in **Figure 1**a and formulated into a facile paddle wheel structure as depicted in Figure 1b.

2.3. Spin-Coating and Thin-Film Formation

2 wt% of synthesized single-crystals of Cu-MOCs were dissolved into ethyl lactate (organic solvent) to form a homogenous solution for spin-coating of thin film as depicted by Figure 1c. This solution was spin-coated on a *p*-type Si (100) substrate to form uniform, large-area, Cu-MOCs thin films, as shown in Figure 1d. Before spin coating, the silicon substrates were cleaned using standard Radio Corporation of America cleanings. Spin-coating was performed at 2100 rpm for 35 s using spin-coater to form uniform thin-films and baked at 95 °C for 1 min to form a thickness of ≈30 nm. The prepared samples were annealed at 70 °C for 20 min to ensure the samples to be free of adsorbate ions and condensed water molecules. Next to this, Figure 1e presents the schematic of large-area uniform Cu-MOCs thin-films deposited on silicon substrates, as shown in Figure 1f. The thickness and dielectric constant of Cu-MOCs thin films are measured through Accurion EP4 Ellipsometer.

2.4. KPFM Charge Injection and Measurements Procedure

AFM (Bruker instruments, model Dimension Icon, USA) was used to characterize Cu-MOCs/Si thin-films surface roughness, morphology, and surface potential, respectively, in the ambient air conditions. To investigate the dielectric response of functional Cu-MOCs thin-films using the KPFM nano-characterization setup as shown in Figure 1g. The setup consisted of AFM topography loop and KPFM feedback loop.[72] The main components of the AFM topography setup included a conducting metal-coated etched antimony-doped silicon probe (MESP) cantilever for probing, monitoring mechanical oscillations, incidence and deflection of the signals through a laser beam and four-quadrant photodetector. The conducting MESP-V2 AFM probe (Bruker) with ≈75 kHz resonant frequency, spring constant 3 N m^{-1}, cantilever thickness ≈2.8 µm, width ≈35 µm, and length ≈225 µm was utilized throughout KPFM investigations. The AFM tip was cleaned using de-ionized water, ethanol, and IPA solvents, followed by nitrogen blow-dry. The topography loop controlled the tip/apex–sample surface distance while applying AC voltage to keep the surface scanning oscillation constant, which was converted to height units to form the surface topography image. The KPFM feedback loop setup mainly consisted of a lock-in amplifier (LIA). A cantilever deflection signal was fed, connecting to a servo controller providing the most necessary feedback loop for data channels. The second loop was mainly used to measure surface potential in which the LIA cancels the mechanical oscillation phase shift of the AC signal by changing the DC tip bias. Each pixel was converted to a color-coded scale to build the electric potential image by nullifying the electric field between tip and sample with the applied DC voltage. For precise measurements, the silicon substrates were grounded for 10 min

Table 1. KPFM surface charge injection and measurement parameters for Cu-MOCs/Si structures.

Nanoscale measurement Parameters	Values
DC bias injection	±3 V
ac bias	500 mV
Probe radius	MESP Co/Cr, ≈40 nm
Spring constant	≈3 N m^{-1}
Probe scan rate	0.99 Hz
Charge injection time	10 min
Line scan	500 nm
Lift Height	≈100 nm
Surface map area	5 μm × 5 μm
Mapping interval	8 min
Measurement Error profile	±5 mV

for any charge saturation. Figure S1a–c, Supporting Information, shows the tapping mode for surface morphology scan before charge injection, KPFM charge injection in contact mode, and KPFM surface potential measurement in non-contact mode with a lift height. The functional Cu-MOCs thin films deposited on silicon substrates showed the surface roughness ≈1.43 ± 0.3 nm, using the surface topology mapping with the scan area of 10 μm × 10 μm. To map the distribution of injected positive and negative charges and monitor the charge retention capacity into Cu-MOCs/Si thin film systems, non-contact 5 μm × 5 μm area scans were conducted. V_{iCPD} was caused by the work function difference of MESP tip (φ_{tip}) and the work function of the silicon (φ_{Si}) substrate,[66] as shown in Figure S2, Supporting Information. Thereby, the surface potential (CPD) maps are obtained through KPFM measurements, which reflect variations in measured surface potentials with the corresponding charge injections on the surface of Cu-MOCs/Si systems. Temporal evolution charge retention was recorded with surface potential (CPD) scan micrographs, captured at fixed time intervals of ≈8 min continuously up to ≈136 min along with a single scan at ≈17 h, respectively. Detailed procedure for KPFM characterization procedure is described in Figure S1 and Section S1, Supporting Information, and the corresponding parameters for KPFM measurement process and operations have been listed in **Table 1**.

2.5. Material Characterizations

The grown single crystals of synthesized Cu-MOCs formulation were characterized using single-crystal X-ray diffraction spectroscopy (SC-XRD, Model-Supernova, Rigaku) as shown in **Figure 2**a. Here, the shown molecular crystal structure contains a paddle wheel-like structure. The dimeric copper was connected with the cluster's four corresponding M-Toluic acid ligands and acetonitrile guest molecule. The Cu-MOCs have a triclinic crystal system, P-1 space group, with the molecular formula of $C_{18}H_{19}CuNO_5$, Cu—Cu distance of ≈2.611 Å, and the cluster size of ≈1.6 nm, that formed a 3D intersecting structure.

Figure 2b shows the top view Field-emission scanning electron microscope (FESEM, Zeiss Gemini 500) image (scale 5 μm) along with Figure 2b-inset, magnified image (scale 10 nm) of Cu-MOCs/Si large-area uniform thin films, and confirms the formation of defect-free uniform thin films. Electron dispersive X-ray spectroscopy was performed using the EDAX, FESEM, Zeiss Gemini 500. The micrograph of EDX measurement confirms the presence of C, O, and Cu constituting elements in Cu-MOCs formulation without any impurities, as shown in Figure 2c. Figure 2c-inset presents tabular data showing the elemental composition and weight percentage of C, O, Cu elements in synthesized Cu-MOCs material. Fourier-transform-infrared-spectroscopy (FTIR) was performed using Agilent Technologies, model-Cary 600 instruments in absorption mode. Figure 2d shows the FTIR spectra of Cu-MOCs to define material properties in the wavenumber ranging from 400 to 4000 cm^{-1} and analyze its surface functional groups. The stretching vibration of the Cu—O bond were recognized at 481.1 $cm^{-1,}$ while the C—H bending of the aromatic ring was recognized between 670 and 750 cm^{-1}. The —C=C bending vibration was observed at 790–920 cm^{-1}. The peaks observed at 1387.7, 1557.5, and 1633.5 cm^{-1}, indicating aromatic C—H stretching, aromatic C=C bending, and —C=C stretching in a cyclic alkene, respectively. The ≈10 μm × 10 μm 2D and 3D tapping mode surface topology AFM micrographs of Cu-MOCs/Si thin-film are shown in Figure 2e,f, respectively, measuring very low surface roughness of ≈1.43 ± 0.3 nm for Cu-MOCs/Si systems, revealing the presence of highly uniform and smooth thin film formation. The top view lateral section MESP-V2 tip FESEM image (scale 30 μm) along with magnified (scale 3 μm) presenting the cantilever and the apex are shown in Figure 2g,i, respectively. The cross-sectional view of the MESP tip reveals a sharp apex, tip radius of ≈40 nm, and the tip height of ≈15 μm, is as shown in Figure 2h, respectively. Hence, by using a sharp apex MESP tip, high-resolution and high-sensitivity AFM images have been successfully demonstrated in the surface potential micrographs of Cu-MOCs/Si structures. The electrostatic response of functional Cu-MOCs dielectric thin film has been successfully shown with high-resolution KPFM measurements along with corresponding (SC-XRD, FESEM, EDX, FTIR, AFM) material characterizations, respectively.

3. Results and Discussion

Figure 3a,b presents the surface potential pattern (CPD) micrographs maps/scans performed by scanning KPFM tip over the Cu-MOCs/Si sample surface. CPD scans closely resemble charge distribution pertaining to distance on the Cu-MOCs/Si sample surface. Due to applied positive (+ve) and negative (–ve) charges, the change in surface potential of Cu-MOCs is also positive (+ve) and negative (–ve), respectively. This indicates in situ transfer of charges to Cu-MOCs rather than the polarization of the dielectric material. Polarization of dielectric causes the polarization charges (+/–) to be opposite in sign than the tip's applied voltage (–/+).[73] Here, the holes and electrons retention/decay in Cu-MOCs is confirmed by the appearance of broad white (bright) contrast spot and wide black (dark) contrast spot on CPD maps, respectively. The positive and negative charges induced Coulomb force on the KPFM cantilever tip to deflect/attract through the trapped holes/electrons in Cu-MOCs/Si surface. It engenders the corresponding elevation and depth contrast profiles watermarked by white and black spots, respectively.

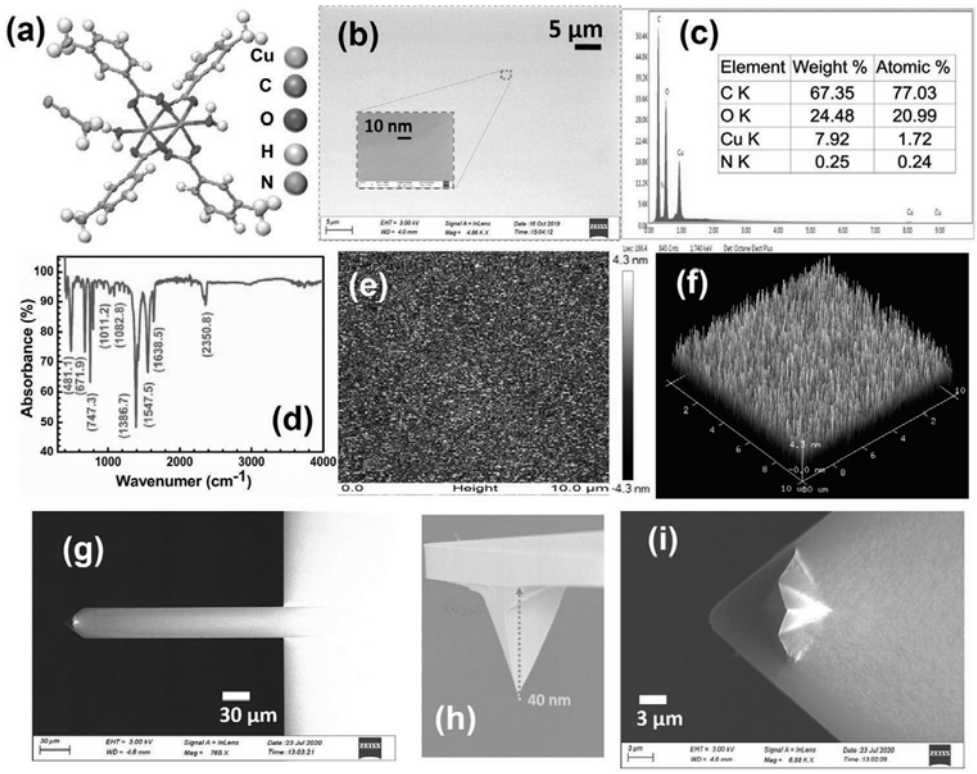

Figure 2. Material characterizations of the synthesized Cu-MOCs crystal structure. a) SC-XRD molecular structure. b) Top view FESEM image of Cu-MOCs/Si thin films at scale 5 µm and (inset) scale 10 nm. c) EDX graph (inset) elemental composition of Cu-MOCs thin-film. d) FTIR spectrum. e) AFM surface topology micrographs obtained from 10 µm × 10 µm surface area in 2D, f) 3D scans with a height profile g) top view FESEM image MESP tip, scale 30 µm, h) side view FESEM image MESP tip, and i) top view FESEM image of MESP tip, scale 3 µm.

For the CPD mapping shown in Figure 3a,b, their corresponding CPD line profiles are obtained through the horizontally scanning of the 2D surface potential map. Figure 3c,d shows the measured holes and electrons CPD values corresponding to the position on the potential map. Estimation of trap charge density (N_t) with the amount of measured CPD can be considered a simple and efficient method of the KPFM technique. This method includes the effects of variation of lift height on the measured CPD values of samples,[15] thickness, and dielectric constant of the dielectric films. It also supports the conducting filament formation hypothesis, which is discussed later in detail. This technique investigates stored charges in the trap sites of Cu-MOCs/Si systems, where total stored charges (Q_S, units: C cm^{-2}) in trap sites is given by $Q_S = C_{eq}(V_{CPD})$.[15,58] Here, C_{eq} is the equivalent capacitance between the MESP tip and surface of the substrate as shown by (Figure S1c, Supporting Information) and given by relation in (Section S1, Supporting Information). As presented by Figure 3c,d V_{CPD} is the measured contact potential difference (CPD) between the MESP tip and Cu-MOCs/Si structures using the AM-KPFM technique, respectively. The total charge density (N_t, units: traps cm^{-2}) stored in trap sites of Cu-MOCs/Si structures can be computed by definition of Q_S and C_{eq} the following relation[15,58] (1):

$$N_t = \frac{V_{CPD}}{e\left[\frac{t_{lift}}{\kappa_{air}} + \frac{t_{CuMOCs}}{\kappa_{CuMOCs}}\right]} \quad (1)$$

where, V_{CPD} is measured CPD potential between the MESP tip and the Cu-MOCs/Si structures, e is the electronic charge, t_{lift} is lift height of MESP tip from the sample, t_{CuMOCs} is thickness of Cu-MOCs thin films onto silicon,[74] κ_{air} is dielectric constant of air and κ_{CuMOCs} is dielectric constant of the high-κ dielectric on to silicon, respectively. **Figure 4**a shows holes and electrons CPD versus time decay plot for the Cu-MOCs/Si structures. This plot is derived from Figure 3 and helps understand overall charge retention/decay statistics in Cu-MOCs/Si structures. Figure 4b shows the plot for computed charge density (N_t) versus time plot to estimate charges density in Cu-MOCs/Si structures. **Figure 5** represents the charge conduction hypothesis through conducting filament model. **Figure 6** shows a comparative analysis of Cu-MOCs dielectric formulations with conventional/high-κ dielectrics.

3.1. Nanoscale Surface Charge Analysis

Figure 3a,b shows surface potential maps for positive and negative charge injection, starting at ≈8 min with a fixed time interval of ≈16 min, respectively. Surface potential maps were recorded continuously up to ≈136 min, and single surface potential maps were recorded at ≈17 h. Figure 3a.1–10,b.1–10 depicts the holes and electrons injection with +3 and −3 V DC bias through the MESP tip for 10 min duration, respectively. With the injection (holes or electrons) of charges, white and black contrast spots are observed onto the surface of Cu-MOCs in successively recorded CPD micrographs. It confirms the

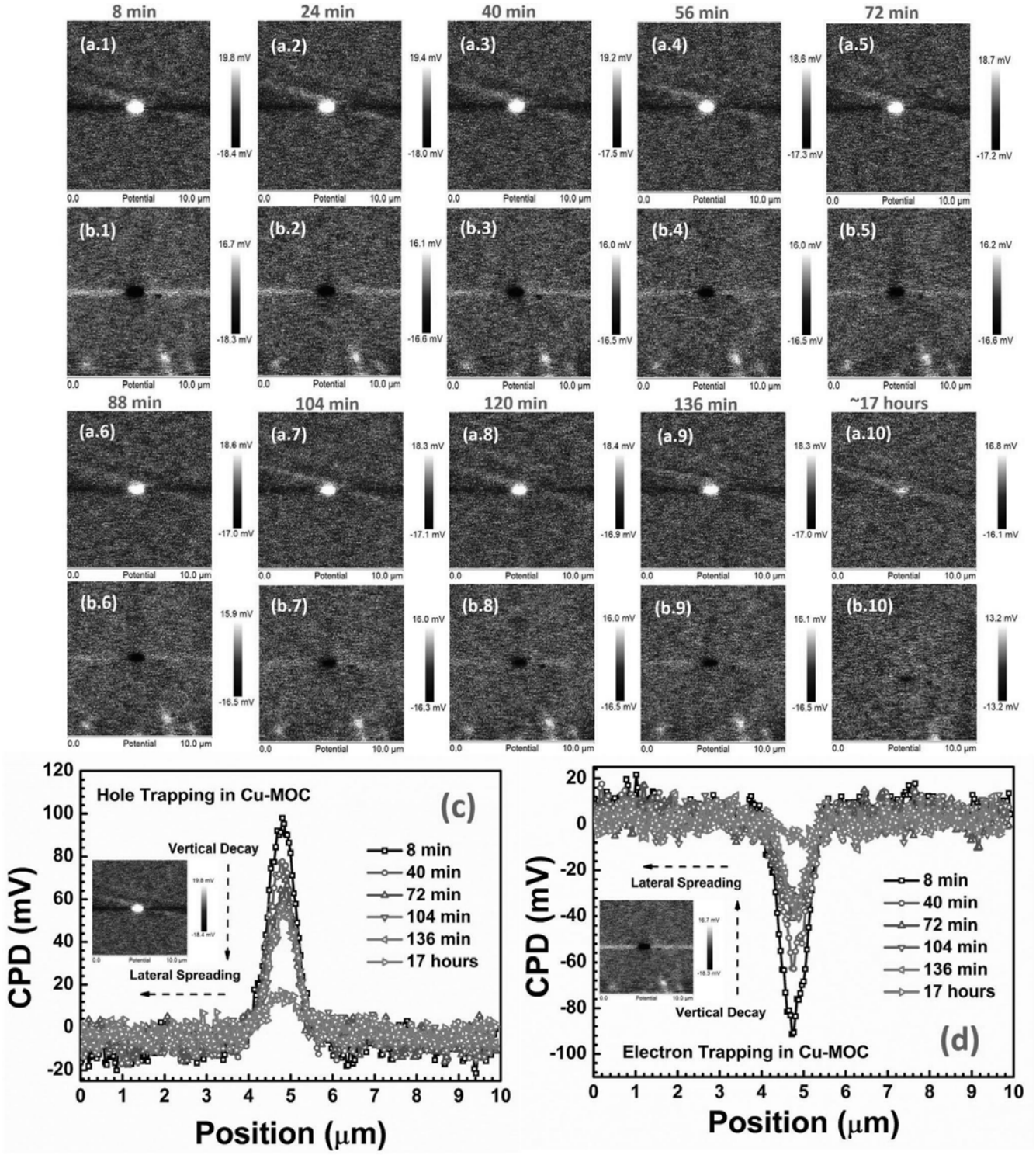

Figure 3. a.1–10,b.1–10) Surface potential holes and electrons CPD scan maps of Cu-MOCs/Si at fixed time intervals (≈32 min) starting ≈8 min up to ≈120 min and a potential scan at 17 h each showing holes and electrons retention and successive decay in CPD by diminishing white and black spots, respectively (c) and (d) holes and electrons CPD retention/decay versus position plot in Cu-MOCs thin film, respectively.

injection/retention (holes and electrons) of charge in the Cu-MOCs/Si system. Successive micrographs reveal a decrease in corresponding white and black contrast spot diameter with the lapse of time.

Figure 3a.1,b.1 shows the maximum CPD contrast spot diameter of ≈1.52 and ≈1.68 μm for holes and electrons, upright CPD recorded at 8 min. Continually, Figure 3a.2–8,b.2–8 shows a further decrease in holes and electrons contact potential contrast

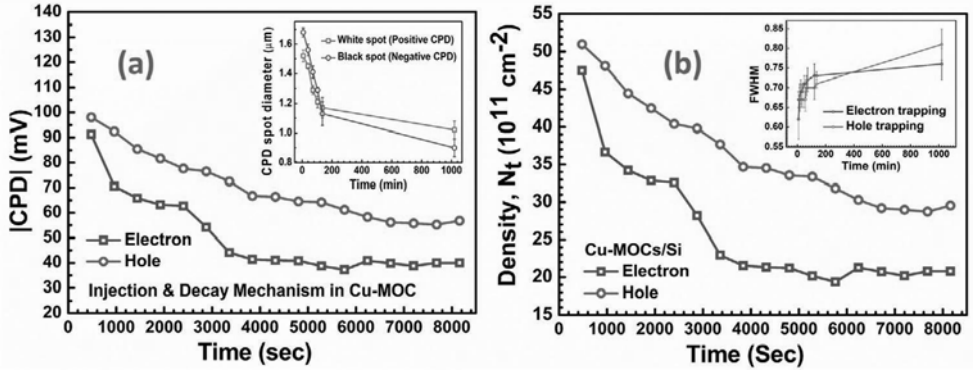

Figure 4. a) Hole and electron CPD decay versus time plot (a-inset) CPD spot diameter versus time plot. b) Total charge (hole and electron) density versus time plot estimated using relation (1), (b-inset) CPD line profile (hole and electron) FWHM versus time plot.

spot diameter. Figure 3a.9,b.9 measured the spot diameters to be ≈1.17 and ≈1.13 μm after 136 min. The slight decrement in holes (≈23%) and electrons (≈32%) spot diameter endorses exceedingly relaxed decay of charge process for Cu-MOCs thin-films. It also indicates holes retention is more favorable than electrons in Cu-MOCs thin films. After that, in Figure 3a.10,b.10, white (≈1.02 μm) and black (≈0.9 μm) contrast spots are observed with resultant (≈68%) and (≈54%) spot diameter after 17 h elapsed, respectively. Nevertheless, even after 17 h of time-lapse, a considerable volume of CPD mapping is still visualized in the Cu-MOCs/Si systems. These contrast spots confirm the gradual decay of retained holes and electrons conduction through Cu-MOCs/silicon interface. Henceforth, the above observations confirm the high charge retention term (more than 17 h) for holes and electrons with a relaxed charge decay process in the Cu-MOCs functional thin films. It justifies the high charge retention ability of functional Cu-MOCs dielectric formulations for reliable gate dielectric in silicon compatible CMOS technology for advanced electronic devices such as MISFETs, tunnel FETs, Fin-FETs, FeRAM, organic-FETs, and sensors.

3.2. Real-Time Surface Charge Probing

Figure 3c,d shows the CPD (mV) line profiles versus position (μm) for the hole and electron injection/retention, respectively. From the CPD mappings, their corresponding CPD line profiles are obtained through horizontal scanning of the 2D surface potential map in non-contact KPFM mode. Figure 3c,d shows that each CPD scan is represented after a fixed time interval of 8 min, 40 min, 72 min, 104 min, 136 min, and a single line profile at 17 h analyze the complete charge decay process. The plots show a proportional decay in hole and electron retention with time for functional Cu-MOCs/Si thin films. Figure 3c-inset,d-inset shows white and black spots surface potential maps corresponding to CPD line profiles at 8 min, respectively.

Primarily after ≈8 min, the maximum CPD is measured to be ≈98 and ≈−91 mV for injected holes and electrons, respectively. Maximum values and sharp contrast line profile of CPD are obtained at (≈4.8 μm) position in Cu-MOCs/Si systems. In Figure 3c,d, past ≈40 min, a marginal decline is observed in the contact potentials ≈77 and ≈−62 mV for holes and electrons,

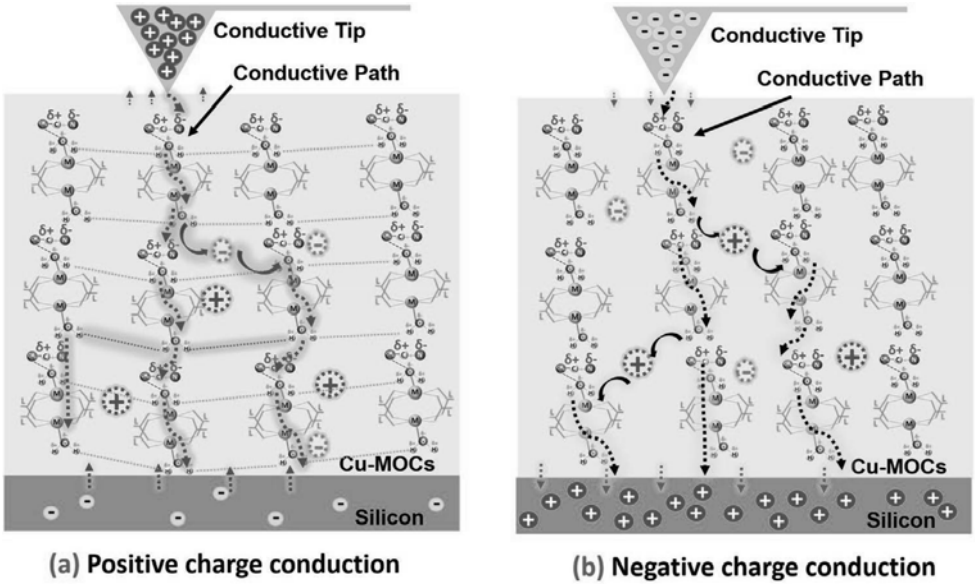

Figure 5. a,b) Positive and negative charge transport through the Cu-MOCs/Si system with conductive filament formation assisted with guest molecule and charge hopping.

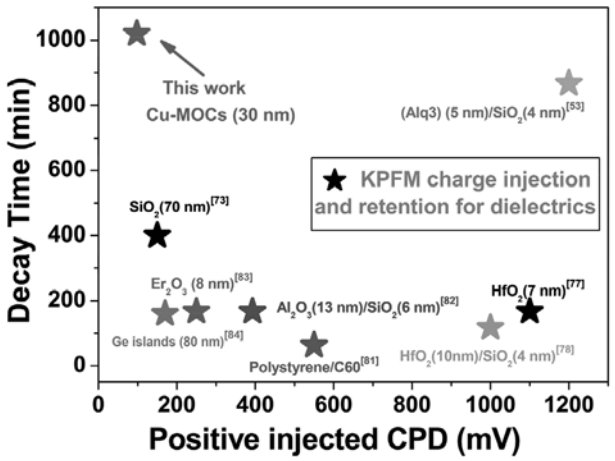

Figure 6. Comparison of conventional dielectrics with Cu-MOCs dielectric formulation for KPFM Charge injection and retention properties.

respectively. CPD line profiles are dignified with largely residual (78%) and (68%) of holes and electrons CPD at 40 min, respectively. Consecutively, 57% and 44% holes and electrons CPD is retained past 72 min time interval, with an outstanding ≈66 and ≈–40 mV holes and electrons CPD contrast line profiles, respectively. Continually after 136 min lapse, CPD contrast line profile peak height declined to ≈56% for electrons and ≈42% for holes, respectively. Moreover, to analyze time for an extensive charge decay, again holes and electrons CPD line profiles are recorded after 17 h, yet to find substantial residual values of contact potential ≈16 and ≈–7 mV, respectively. Therefore simply 84% and 92% of total charge (holes and electrons) decay after 17 h, indicate a retention time of more than 17 h required to decay the injected charges in Cu-MOCs thin films entirely. It demonstrates that holes injection and holes retention are favorable compared to electrons in the functional Cu-MOCs/Si system. Henceforth, the above observations indicate a high charge retention ability of more than 17 h in Cu-MOCs/Si systems for holes and electrons-based majority carrier electronics.

3.3. Positive versus Negative Surface Charges Study

Figure 4a shows |CPD| (mV) versus decay time (s) plot for the injected hole and electron charge carriers in the Cu-MOC/Si system. The absolute values of |CPD| for holes and electrons charge carriers decay exponentially with time-varying from 480 to 8160 s at a fixed interval of 480 s, respectively. Maximum magnitudes of |CPD| obtained at (≈4.8 μm) position in surface potential maps are used in all calculations. With the positive and negative charges retention mechanisms assumed to be similar, an injection offset and Fermi level alignment between positive and negative charges are observed to be ≈190 mV. It is noticed that the |CPD| values of the holes (red curve) and electrons (blue curve) decrease swiftly with time. In Figure 4a, after 1440 s, almost 87% and 74% of holes and electrons CPD is effectively retained in Cu-MOCs/Si systems. Correspondingly, 71% and 48% of holes and electrons charges are retained after 3360 s of CPD measurements. It is observed that 62% positive and 50% negative charges are retained over the first 4000 s. After the first 4000 s, the charge decay process becomes further relaxed and loses the residual charges moderately by the end of 8160 s. After that, 57% of positive charges and 38% of negative charges are retained after 8160 s. Noteworthy, the retention time of holes is longer than that of electrons, as discussed in Section 3.2. It is noticed that with the application of the same magnitude (3 V) of positive and negative DC potential, the CPD peak magnitude for injected positive charges are slightly (≈7 mV) higher than that of the injected negative charges in Cu-MOCs. This directs that the holes injection quantity is higher and favorable than electrons. The more considerable potential barrier height of Cu-MOCs/Si system than its potential well depth may cause the longer retention of holes than that of electrons.[70] Henceforth, holes retention is favorable, enlightened through the asymmetric conductance and valance band offset at the Cu-MOC/Si interface.[70]

Furthermore, Figure 4a-inset shows CPD spot diameter versus time plot for Cu-MOCs/Si structures. The plot is presented at fixed intervals 8, 40, 72, 104, 136, 1020 min. A decrease in the diameter of white and black contrast spots is observed from (1.52 ± 0.04, 1.17 ± 0.07 to 1.02 ± 0.06 μm) and (1.68 ± 0.03, 1.13 ± 0.08 to 0.09 ± 0.06 μm) at 8, 136, and 1020 min, respectively. The reduction in spot size is slight, confirming long-term charge retention and relaxed charge decay in Cu-MOCs/Si structures. Reduction in spot size also confirms the presence of lateral dispersion of charges in Cu-MOCs/Si systems.[75] Additionally, the decrease ≈0.55 μm in CPD contrast spot diameter of electrons is greater than that of hole CPD spot diameter ≈0.35 μm. This evidence attributes that the positive charge retention into the Cu-MOCs/Si system is much higher than negative charges. It rationalizes the potential candidacy of Cu-MOCs/Si systems for its long-term charge retention and relaxed charge decay for the futuristic high-performance dielectric applications in next-generation FETs technology.

3.4. Surface Charge Density Calculations

Figure 4b shows the plot of trapped charge density (N_t) as a function of time (≈8000 s) for both charges (red curve for holes) and (blue curve for electrons) for the Cu-MOCs/Si systems. The value of trapped (holes) charge density, $N_{t,h}$, and (electrons) charge density, $N_{t,e}$, are calculated using the Equation (1) as stated in Section 3. $N_{t,h}$, and $N_{t,e}$ values are computed from 480 to 8160 s, with the fixed time interval of 480 s, respectively. Maximum |CPD| magnitudes at (≈4.8 μm) position of the surface potential map are used in all calculations. $N_{t,h}$, and $N_{t,e}$ are calculated as $\approx 5.09 \times 10^{12}$ and $\approx 4.44 \times 10^{12}$ traps cm^{-2}; $\approx 2.95 \times 10^{12}$ and $\approx 4.74 \times 10^{12}$ traps cm^{-2}; $\approx 3.42 \times 10^{12}$ and $\approx 2.07 \times 10^{12}$ traps cm^{-2} at 480, 1440, and 8160 s, respectively. As evident from Figure 4b, the holes trapped charge density decays slowly compared to electrons, in line with the discussion in Section 3.3. This indicates holes retention is favorable than electrons in Cu-MOCs/Si systems. Moreover, the high remnant trapped charge density of holes and electrons after ≈8000 s of CPD measurements indicates long-term charge retention and relaxed charges decay in Cu-MOCs/Si thin-film.

Figure 4b-inset shows the FWHM of CPD line profile (hole and electron) versus time plot for Cu-MOCs/Si systems. The

plot is presented at fixed intervals 8, 40, 72, 104, 136, 1020 min. The plot shows an increase in FWHM of surface potential CPD line profile with the progress of time. Holes and electrons FWHM of CPD line profile at 8, 136, 1020 min is (0.67 ± 0.04, 0.71 ± 0.01, 0.81 ± 0.04) and (0.62 ± 0.05, 0.73 ± 0.01, 0.76 ± 0.04), respectively. This slow increase in FWHM indicates a highly relaxed decay of charges in Cu-MOCs/Si systems. Also, an increase in FWHM of electrons CPD is more prominent than that of holes. It indicates holes retention is favorable than electrons in Cu-MOCs thin films. In Figure 4a-inset,b-inset, the decrease in holes and electrons CPD spot diameter (≈23%) and (≈32%) is more significant than their increase in FWHM (≈6%) and (≈16%), respectively as per discussion in Section 3.3. It authorizes that the charge decay is predominantly relaxed in both downward/vertical and sideways/lateral charge transport directions in Cu-MOCs/Si systems.[75] Thus, the Cu-MOCs/Si structures depict long-term charge retention ability with relaxed multi-directional decay mechanisms, proving their potential candidature as an alternate, high-κ dielectric for future FETs applications.

3.5. Charge Conduction Mechanism

Meanwhile, for the case of Cu-MOCs adsorbing small molecules through host–guest interactions, trapping, retention, and decay performance can be chemically modulated. It exhibits its potential to overcome the gap between chemical information and electrical properties. The phenomenon of charge injection, retention, and decay is further explained by the transport of positive and negative charges through the vertical conduction/decay with the formation of conductive least resistance paths. These conductive paths are majorly assisted by the presence of guest molecules in the Cu-MOCs clusters along with the aid of fixed and mobile ions charges. All intrinsic charges are assumed to be uniformly distributed in the sample before charge injection. Hence, the presence of intrinsic charges is irrelevant to that of injected charges and can be eliminated in the CPD measurements.[32] Cu-MOCs being intrinsically nano-porous, presence of nanocrystalline domains, discrete structures, charges may be trapped/retained between the two or more discontinuous clusters.[75–78] A single Cu-MOCs cluster unit is shown in (Figure S3, Supporting Information) consisting of acetonitrile (CH_3CN) solvent group as a guest molecule attached with adjacent clusters. Due to the presence of polar covalent bond of C–N in CH_3CN guest molecule, weak partial negative and positive charges exist on the N and C atoms, respectively. Similarly, polar covalent O–H bond,[79] partial negative and positive charge exists on O and H atoms, respectively. Also, the discrete Cu-MOCs clusters are attached to each other through weak H–H (hydrogen) bonds. In this support, a vertical conductive filament model is proposed, as shown in Figure 5a,b. In Figure 5a, positive bias is applied on Cu-MOCs/Si system, and holes are injected on the surface of Cu-MOCs at the air/Cu-MOCs interface. Consequently, the injected positive charges are initially accumulated and retained at the surface of Cu-MOCs. Next, temporal evolution positive charges are attracted to the partial negative charges present on the N atom in CH_3CN solvent group and also attracted to the closely lying partially negative O atoms of O—H bond in the Cu-MOCs cluster as shown in (Figure S3, Supporting Information). Continually, the positive charges may jump/hop from one cluster to adjacent cluster through charge hopping via the negatively charged mobile ions present in the Cu-MOCs/Si systems. Moreover, the positive charges may escort from one cluster to adjacent cluster through the weak H—H proton conduction through lateral dispersion.[77,80] Hence, the above mechanisms provide much longer pathways for the positive charges to approach Si substrate, justifying favorable holes retention compared to electrons, as in line with the discussion in Section 3.3. Conclusively, a single conductive path's branching leads to multiple exits for surface charges to approach the underlying silicon substrate.

Similar behavior occurs when the negative bias is applied through the AFM tip, and electrons are injected on Cu-MOCs/Si system, as shown in Figure 5b. The injected negative charge is mainly transported through the presence of partial positive charges on the C atom in C—N bonds and through H atoms in O—H bonds. The negative charge may be conducted laterally by the charge hopping process with fixed positive oxide charges present in the Cu-MOCs/Si systems.[77,78] Hence, the charge decay mechanism in Cu-MOCs/Si system is well-understood with the conductive path filament mechanism. The corresponding band-bending diagram of Cu-MOCs/Si system with +3 and −3 V charge injection is shown in Figure S4a,b, Supporting Information, respectively.

Comparative measurement parameters for holes and electrons charge retention/decay obtained from KPFM mapping onto Cu-MOCs/Si structures are listed in **Table 2**.

Figure 6 compares conventional dielectrics, or a combination of dielectrics with Cu-MOCs dielectric formulation for KPFM charge injection and retention properties.[30,53,73,77,78,81–83] Figure 6 shows a positive CPD (mV) versus decay time (min) plot for Cu-MOCs, SiO_2,[73] Er_2O_3,[30] Al_2O_3,[82] HfO_2,[77] polystyrene/C60,[81] Alq3,[53] Ge islands,[83] combination of dielectrics,[78] etc. Cu-MOCs show that with a low CPD injection ≈98 mV, high charge retention ≈1020 min is observed. However, high-κ dielectrics such as HfO_2, Al_2O_3 even with high CPD injections, show much lower retention times. Whereas, SiO_2, Er_2O_3, and Ge islands having comparably low CPD injections show lower retention times consequently. Hence, Cu-MOCs having low charge injections show the best retention time among dielectrics listed above. Therefore, Cu-MOCs prove their competency toward high-κ dielectrics for next-generation FETs.

Table 2. List of conclusive KPFM measurements of this work (Cu-MOCs/Si) structures.

This work	Parameter Values	
Cu-MOCs/Si structures	Holes	Electrons
CPD (@ 8 min)	≈98 mV	≈−91 mV
CPD spot diameter @8 min	≈1.52 µm	≈1.68 µm
Charge density	5.09×10^{12} cm^{-2}	4.74×10^{12} cm^{-2}
% Charge decay after 17 h	84%	92%
Cu-MOCs Surface roughness	≈1.43 ± 0.3 nm	
Cu-MOCs Dielectric Thickness	≈30 nm	
Unit Cluster size	≈1.6 nm	

4. Conclusions

A novel Cu-MOCs nanostructures formulation is developed using the sol–gel method. It dissolves homogeneously in organic solvents to make uniform thin films on the Si substrates. Nanoscale investigations of surface charges retention/decay and electronic properties are probed for Cu-MOCs/Si systems by non-destructive AM-KPFM. Cu-MOCs are suitable for futuristic electronic applications such as MISFETs, FeRAM, NVM, tunnel FETs, organic-FETs, Fin-FETs, and sensor devices. Consecutively, holes and electrons charges are injected on Cu-MOCs/Si systems through positive and negative potential DC biases, respectively. The presence of white and black contrast profiles spots confirms the charge injection, retention, and subsequent decay of CPD. The surface charge study demonstrates long-term hole and electron charge retention in Cu-MOCs/Si systems and the relaxed decay of corresponding charges through the underlying silicon substrate, as elucidated through a conductive filament model of Cu-MOCs/Si systems. Hence, KPFM based CPD investigations on novel synthesized Cu-MOCs/Si structures paving the way toward a better understanding of organic–inorganic materials for the futuristic silicon compatible CMOS electronic, optoelectronic, photovoltaic devices for next-generation technology nodes.

Supporting Information

Supporting Information is available from the Wiley Online Library or from the author.

Acknowledgements

The authors thank the Department of Science and Technology (DST) India for financial support. The authors would like to strongly acknowledge the Centre for Design and Fabrication of Electronic Devices (C4DFED), and Advanced Materials Research Centre (AMRC), Indian Institute of Technology (IIT) Mandi, India, for the use of various state-of-the-art device fabrication and characterization facilities for this work. P.G. would like to thank 'INSPIRE Ph.D. Fellowship Program (Research Fellowship-IF180505) support from the Department of Science and Technology (DST) Govt. of India. R.K. thanks the Science and Engineering Research Board (SERB) New Delhi, India, for the national postdoc fellowship (Sanction Project reference number: PDF/2017/001437).

Conflict of Interest

The authors declare no conflict of interest.

Data Availability Statement

Research data are not shared.

Keywords

charge retention, filament conduction, Kelvin probe force microscopy, metal–insulator–semiconductors, metal–organic clusters, surface potential

Received: April 3, 2021
Revised: August 6, 2021
Published online: September 26, 2021

[1] H. Furukawa, K. E. Cordova, M. O'keeffe, O. M. Yaghi, *Science* **2013**, *341*, 1230444.
[2] H.-C. J. Zhou, S. Kitagawa, *Chem. Soc. Rev.* **2014**, *43*, 5415.
[3] L. S. Xie, G. Skorupskii, M. Dincă, *Chem. Rev.* **2020**, *120*, 8536.
[4] J. L. C. Rowsell, O. M. Yaghi, *Microporous Mesoporous Mater.* **2004**, *73*, 3.
[5] J. A. Mason, M. Veenstra, J. R. Long, *Chem. Sci.* **2014**, *5*, 32.
[6] Y. Zhao, Z. Song, X. Li, Q. Sun, N. Cheng, S. Lawes, X. Sun, *Energy Storage Mater.* **2016**, *2*, 35.
[7] J. Lee, O. K. Farha, J. Roberts, K. A. Scheidt, S. T. Nguyen, J. T. Hupp, *Chem. Soc. Rev.* **2009**, *38*, 1450.
[8] J.-R. Li, J. Sculley, H.-C. Zhou, *Chem. Rev.* **2012**, *112*, 869.
[9] M. K. Smith, K. A. Mirica, *J. Am. Chem. Soc.* **2017**, *139*, 16759.
[10] Z.-G. Gu, S.-C Chen, W.-Q. Fu, Q. Zheng, J. Zhang, *ACS Appl. Mater. Interfaces* **2017**, *9*, 7259.
[11] A. Pathak, G. R. Chiou, N. R. Gade, M. Usman, S. Mendiratta, T.-T. Luo, T. W. Tseng, J.-W. Chen, F.-R. Chen, K.-H. Chen, L.-C. Chen, K.-L. Lu, *ACS Appl. Mater. Interfaces* **2017**, *9*, 21872.
[12] W.-J. Li, J. Liu, Z.-H. Sun, T.-F. Liu, J. Lü, S.-Y. Gao, C. He, R. Cao, J.-H. Luo, *Nat. Commun.* **2016**, *7*, 11830.
[13] S. Eslava, L. Zhang, S. Esconjauregui, J. Yang, K. Vanstreels, M. R. Baklanov, E. Saiz, *Chem. Mater.* **2013**, *25*, 27.
[14] C. Yang, R. Dong, M. Wang, P. S. Petkov, Z. Zhang, M. Wang, P. Han, M. Ballabio, S. A. Bräuninger, Z. Liao, J. Zhang, F. Schwotzer, E. Zschech, H.-H. Klauss, E. Cánovas, S. Kaskel, M. Bonn, S. Zhou, T. Heine, X. Feng, *Nat. Commun.* **2019**, *10*, 3269.
[15] J. Duan, S. Chen, C. Zhao, *Nat. Commun.* **2017**, *8*, 1.
[16] H. Manjunatha, K. C. B. Naidu, N. S. Kumar, R. Pothu, R. Boddula, in *Applications of Metal–Organic Frameworks and Their Derived Materials* (Eds: I. Inamuddin, R. Boddula, M. I. Ahamed, A. M. Asiri), Wiley, New York **2020**, p. 33.
[17] Q. Fu, Y. Ran, X. Zhang, J. Ge, *ACS Appl. Mater. Interfaces* **2020**, *12*, 44058.
[18] M. Usman, S. Mendiratta, K.-L. Lu, *Adv. Mater.* **2017**, *29*, 1605071.
[19] P. Jain, A. Stroppa, D. Nabok, A. Marino, A. Rubano, D. Paparo, M. Matsubara, H. Nakotte, M. Fiebig, S. Picozzi, E. S. Choi, A. K. Cheetham, C. Draxl, N. S. Dalal, V. S. Zapf, *npj Quantum Mater.* **2016**, *1*, 16012.
[20] R. Dong, Z. Zhang, D. C. Tranca, S. Zhou, M. Wang, P. Adler, Z. Liao, F. Liu, Y. Sun, W. Shi, Z. Zhang, E. Zschech, S. C. B. Mannsfeld, C. Felser, X. Feng, *Nat. Commun.* **2018**, *9*, 2637.
[21] M. Suyetin, T. Heine, *J. Mater. Chem. C* **2020**, *8*, 1567.
[22] G. Wu, J. Huang, Y. Zang, J. He, G. Xu, *J. Am. Chem. Soc.* **2017**, *139*, 1360.
[23] L. M. Montañez, K. Müller, L. Heinke, H. J Osten, *Microporous Mesoporous Mater.* **2018**, *265*, 185.
[24] G. A. Bodkhe, M. A. Deshmukh, H. K. Patil, S. M. Shirsat, V. Srihari, K. K. Pandey, G. Panchal, D. M. Phase, A. Mulchandani, M. D. Shirsat, *J. Phys. D: Appl. Phys.* **2019**, *52*, 335105.
[25] A. Saeidi, T. Rosca, E. Memisevic, I. Stolichnov, M. Cavalieri, L.-E. Wernersson, A. M. Ionescu, *Nano Lett.* **2020**, *20*, 3255.
[26] S. Yuvaraja, S. G. Surya, M. T. Vijjapu, V. Chernikova, O. Shekhah, M. Eddaoudi, K. N. Salama, *Phys. Status Solidi RRL* **2020**, *14*, 2000086.
[27] D. Caimi, M. Sousa, S. Karg, C. B. Zota, *Jpn. J. Appl. Phys.* **2021**, *60*, SB0801.
[28] D. W. Gardner, X. Gao, H. M. Fahad, A.-T. Yang, S. He, A. Javey, C. Carraro, R. Maboudian, *Chem. - Eur. J.* **2019**, *25*, 13176.

[29] International Technology Roadmap for Semiconductors. **2020**.
[30] R. Khosla, P. Kumar, S. K. Sharma, *IEEE Trans. Device Mater. Reliab.* **2015**, *15*, 610.
[31] S. M. Yoon, S. C. Warren, B. A. Grzybowski, *Angew. Chem.* **2014**, *126*, 4526.
[32] Z. Wang, D. Nminibapiel, P. Shrestha, J. Liu, W. Guo, P. G. Weidler, H. Baumgart, C. Wöll, E. Redel, *ChemNanoMat* **2016**, *2*, 67.
[33] M. Usman, S. Mendiratta, K.-L. Lu, *ChemElectroChem* **2015**, *2*, 786.
[34] A. I. Inamdar, A. Pathak, M. Usman, K.-R. Chiou, P.-H. Tsai, S. Mendiratta, S. Kamal, Y.-H. Liu, J.-W. Chen, M.-H. Chiang, K.-L. Lu, *J. Mater. Chem. A* **2020**, *8*, 11958.
[35] V. Stavila, A. A. Talin, M. D. Allendorf, *Chem. Soc. Rev.* **2014**, *43*, 5994.
[36] C.-C. Chueh, C.-I. Chen, Y.-A. Su, H. Konnerth, Y.-J. Gu, C.-W. Kung, K. C.-W. Wu, *J. Mater. Chem. A* **2019**, *7*, 17079.
[37] D. M. D'alessandro, *Chem. Commun.* **2016**, *52*, 8957.
[38] J. Su, S. Yuan, H.-Y. Wang, L. Huang, J.-Y. Ge, E. Joseph, J. Qin, T. Cagin, J.-L. Zuo, H.-C. Zhou, *Nat. Commun.* **2017**, *8*, 2008.
[39] P. Li, Bo Wang, *Isr. J. Chem.* **2018**, *58*, 1010.
[40] L. Sun, M. G. Campbell, M. Dincă, *Angew. Chem., Int. Ed.* **2016**, *55*, 3566.
[41] M. Ko, L. Mendecki, K. A. Mirica, *Chem. Commun.* **2018**, *54*, 7873.
[42] S. Galli, A. Cimino, J. F. Ivy, C. Giacobbe, R. K. Arvapally, R. Vismara, S. Checchia, M. A. Rawshdeh, C. T. Cardenas, W. K. Yaseen, A. Maspero, M. A. Omary, *Adv. Funct. Mater.* **2019**, *29*, 1904707.
[43] S. Goswami, D. Ray, K.-I. Otake, C.-W. Kung, S J. Garibay, T. Islamoglu, A. Atilgan, Y. Cui, C. J. Cramer, O. K. Farha, J. T. Hupp, *Chem. Sci.* **2018**, *9*, 4477.
[44] C.-W. Kung, K. Otake, C. T. Buru, S. Goswami, Y. Cui, J. T. Hupp, A. M. Spokoyny, O. K. Farha, *J. Am. Chem. Soc.* **2018**, *140*, 3871.
[45] M. Usman, P.-H. Feng, K.-R. Chiou, J.-W. Chen, L.-W. Lee, Y.-H. Liu, K.-L. Lu, *ACS Appl. Electron. Mater.* **2019**, *1*, 836.
[46] E. Redel, Z. Wang, S. Walheim, J. Liu, H. Gliemann, C. Wöll, *Appl. Phys. Lett.* **2013**, *103*, 091903.
[47] M. J. Deen, F. Pascal, in *Electrical Characterization of Semiconductor Materials and Devices BT–Springer Handbook of Electronic and Photonic Materials* (Eds: S. Kasap, P. Capper), Springer International Publishing, New York **2017**, 1.
[48] Y. Z. Zhu, Z. Zhu, Z. M. Yin, Z. D. Xiang, *J. Mater. Sci. Technol.* **2009**, *25*, 989.
[49] D. S. Jakob, H. Wang, X. G. Xu, *ACS Nano* **2020**, *14*, 4839.
[50] K. Byrne, A. Shik, D. Wisniewski, H. E. Ruda, *Small* **2020**, *16*, 1907321.
[51] T. Coffey, A. Seredinski, J. N. Poler, C. Patteson, W H. Watts, K. Baptiste, C. Zheng, J. Cody, C. J. Collison, *Thin Solid Films* **2019**, *669*, 120.
[52] *Metrology and Diagnostic Techniques for Nanoelectronics* (Eds: Z. Ma, D. G. Seiler), Jenny Stanford Publishing, New York **2016**.
[53] S. Paydavosi, K. E. Aidala, P. R. Brown, P. Hashemi, G. J. Supran, T. P. Osedach, J. L. Hoyt, V. Bulović, *Nano Lett.* **2012**, *12*, 1260.
[54] M. Ishii, *J. Phys.: Condens. Matter* **2010**, *22*, 173001.
[55] C. A. Rezende, R. F. Gouveia, M. A. Silva, F. Galembeck, *J. Phys.: Condens. Matter* **2009**, *21*, 263002.
[56] C. Villeneuve-Faure, L. Boudou, K. Makasheva, G. Teyssedre, *Nanotechnology* **2017**, *28*, 505701.
[57] M. Vishwakarma, D. Varandani, M. Hendrickx, J. Hadermann, B. R. Mehta, *Mater. Res. Express* **2020**, *7*, 016418.
[58] L. Huang, D. Zhang, S. Bu, R. Peng, Q. Wei, Z. Ge, *Adv. Sci.* **2020**, *7*, 1902656.
[59] P. Sharma, D. Sando, Q. Zhang, X. Cheng, S. Prosandeev, R. Bulanadi, S. Prokhorenko, L. Bellaiche, L.-Q. Chen, V. Nagarajan, J. Seidel, *Adv. Funct. Mater.* **2019**, *29*, 1807523.
[60] B. Vasić, S. Aškrabić, M. M. Jakovljević, M. Artemyev, *Appl. Surf. Sci.* **2020**, *513*, 145822.
[61] C.-C. Tsai, H.-H. Hung, C.-P. Liu, Y.-T. Chen, C.-Y. Pan, *PLoS One* **2012**, *7*, e33849.
[62] H. Ryu, J.-H Lee, T.-Y. Kim, U. Khan, J. H. Lee, S. S. Kwak, H.-J. Yoon, S.-W. Kim, *Adv. Energy Mater.* **2017**, *7*, 1700289.
[63] Y. Zhang, D. Ziegler, M. Salmeron, *ACS Nano* **2013**, *7*, 8258.
[64] H. Xie, H. Zhang, D. Hussain, X. Meng, J. Song, L. Sun, *Langmuir* **2017**, *33*, 2725.
[65] Y. Wang, Z. Hu, C. Gao, C. Yang, J. Zhang, Y. Zhu, *Adv. Mater. Interfaces* **2020**, *7*, 1901521.
[66] L. Collins, J. I. Kilpatrick, S. V. Kalinin, B. J. Rodriguez, *Rep. Prog. Phys.* **2018**, *81*, 086101.
[67] Z. Kang, H. Si, M. Shi, C. Xu, W. Fan, S. Ma, A. Kausar, Q. Liao, Z. Zhang, Y. Zhang, *Sci. China Mater.* **2019**, *62*, 776.
[68] A. Axt, I. M. Hermes, V. W. Bergmann, N. Tausendpfund, S. A. L. Weber, *Beilstein J. Nanotechnol.* **2018**, *9*, 1809.
[69] C. Dumas, L. Ressier, J. Grisolia, A. Arbouet, V. Paillard, G. Benassayag, S. Schamm, P. Normand, *Microelectron. Eng.* **2008**, *85*, 2358.
[70] J. Xu, J. Xu, P. Zhang, W. Li, K. Chen, *Nanoscale* **2013**, *5*, 9971.
[71] J. Xu, J. Xu, P. Lu, D. Shan, W. Li, K. Chen, *J. Appl. Phys.* **2014**, *116*, 134309.
[72] H. Lee, W. Lee, J. H. Lee, D. S. Yoon, *J. Nanomater.* **2016**, *2016*, 4209130.
[73] C. Maedler, H. Graaf, *J. Phys. Chem. C* **2013**, *117*, 5358.
[74] P. Gupta, R. Kumar, S. K. Sharma, *Adv. Electron. Mater.* **2021**, *7*, 2000835.
[75] S. - D. Tzeng, S. Gwo, *J. Appl. Phys.* **2006**, *100*, 023711.
[76] L. G. Kaake, P. F. Barbara, X.-Y. Zhu, *J. Phys. Chem. Lett.* **2010**, *1*, 628.
[77] G. Liu, W. Jiang, J. Zhu, W. Cao, *Appl. Phys. Lett.* **2011**, *99*, 162901.
[78] Y. Han, Z. Huo, X. Li, G. Chen, X. Yang, D. Zhang, Y. Wang, T. Ye, M. Liu, *IEEE Electron Device Lett.* **2013**, *34*, 870.
[79] A. J. Rieth, K. M. Hunter, M. Dincă, F. Paesani, *Nat. Commun.* **2019**, *10*, 4771.
[80] J. Su, W. He, X.-M. Li, L. Sun, H.-Y. Wang, Y.-Q. Lan, M. Ding, J.-L. Zuo, *Matter* **2020**, *2*, 711.
[81] J. Wang, X. Wang, J.-J. Xu, L.-H. Xie, M.-D. Yi, W. Huang, *Org. Electron.* **2017**, *44*, 247.
[82] R. Khosla, E. G. Rolseth, P. Kumar, S. S. Vadakupudhupalayam, S. K. Sharma, J. Schulze, *IEEE Trans. Device Mater. Reliab.* **2017**, *17*, 80.
[83] Z. Lin, P. Brunkov, F. Bassani, G. Bremond, *Appl. Phys. Lett.* **2010**, *97*, 263112.

